EVOLUTION OF CIRCULAR POLARIZATION RATIO (CPR) PROFILES OF KILOMETER-SCALE CRATERS ON THE LUNAR MARIA. I. R. King[1], C. I. Fassett[2], B. J. Thomson[3], D. A. Minton[4], W. A. Watters[5]. [1]Harvey Mudd College, Claremont, CA 91711 (iking@g.hmc.edu), [2]NASA Marshall Space Flight Center, Huntsville, AL 35805, [3]Dept. of Earth and Planetary Sciences, University of Tennessee, Knoxville, TN 37922, [4] Dept. of Earth, Atmospheric, and Planetary Science, Purdue University, West Lafayette, IN 47907· , [5]Dept. of Astronomy, Wellesley College, Wellesley, MA 02481.

Introduction: When sufficiently large impact craters form on the Moon, rocks and unweathered materials are excavated from beneath the regolith and deposited into their blocky ejecta [1]. This enhances the rockiness and roughness of the proximal ejecta surrounding fresh impact craters [2-5]. The interior of fresh craters are typically also rough, due to blocks, breccia, and impact melt [6]. Thus, both the interior and proximal ejecta of fresh craters are usually radar bright and have high circular polarization ratios (CPR) [7]. Beyond the proximal ejecta, radar-dark halos are observed around some fresh craters, suggesting that distal ejecta is finer-grained than background regolith [8]. The radar signatures of craters fade with time [e.g., 2,3,9] as the regolith grows.

New impacts have occurred steadily since the formation of the maria, and craters are found superposed on the maria with a wide range of ages. Thus, examining the CPR of these impact craters allows us to directly explore the rates and processes of regolith evolution. We used the ~15 m/px S-band (12.6 cm) Zoom radar observations obtained by the Mini-RF instrument on the Lunar Reconnaissance Orbiter [10,11] and extracted CPR profiles of a large population of kilometer-scale craters. S-band CPR is sensitive to rocks and roughness at a length scale of the wavelength of the radar (i.e., decimeter scales) [e.g., 12]. The goal of this study was to explore the relationship between CPR signatures and crater age on the lunar maria.

Data and Methodology: The craters we examined are from an existing dataset of >13,000 craters on the maria, ranging 800 m to 5 km in diameter, with previously determined degradation states and age estimates based on their topography [12]. These craters were manually co-registered to Mini-RF level 2 observations from the PDS, and for each crater, radial CPR profiles were extracted. In total, we analyzed 6,056 crater observations, which included 5,142 unique craters covered by a single Mini-RF S-band zoom swath and 914 craters covered by multiple Mini-RF swaths. Repeat measurements in this latter group of craters enabled us to assess uncertainties in CPR profiles.

Craters were analyzed by constructing median radial profiles of individual craters (e.g., Fig. 1), as well as median profiles of groups of craters combined by age and diameter. These groupings enabled us to characterize how CPR evolves with degradation state (age) as a function of time (e.g., Fig. 2). Constructing median radial profiles across multiple azimuths around the crater partially mitigates speckle noise, but throws out information about azimuthal variability. Likewise, the median profiles of groups of observations further reduces variability; however, it requires assuming that craters of a given size and age on the maria evolved similarly.

Results: Figure 2 shows the general evolution of CPR for the km-scale craters (limited to the 3,942 craters between 800m and 1.2 km). For fresh craters ($\kappa t<6000$, t<~500 Ma old), CPR profiles often have a local maxima just outside the crater rim (R~1.1 to 1.2). That this maxima falls slightly beyond the topographic rim (R=1) is not surprising, as direct measurements of rock distributions show enhanced boulder densities in these areas as well [e.g., 14].

The CPR of distal ejecta deposits beyond ~1.5 R evolve monotonically from higher CPR to lower CPR with time, reaching the background value of the surrounding maria over approximately ~2 Ga for craters in the 800 m to 1.2 km diameter range. The decrease in CPR with time outside the craters' rims is attributed to the elimination of rocks in the ejecta as the regolith grows. (Note that CPR observations in the ejecta of larger craters (~2 to 5 km, and above), return to background values more slowly, both in the larger data set we analyzed and in earlier work [e.g., 7]).

The interior behavior of km-scale craters is more complicated. Typically the CPR of the central crater interiors appear to increase before starting to decline. We hypothesize that the reason for this initial increase may be ongoing transport of rocks from the steep slopes of the rim and upper crater walls to the crater floor, a process that can continue long after crater formation. Fig. 2 implies that, on average, decimeter-scale rocks are delivered to the central crater floor faster than they are destroyed and/or buried for the first ~500 Ma. After ~500 Ma, this process reverses, and the rocks enhancing CPR inside the crater begin are increasingly destroyed or buried to depths greater than tens of cm. The observed CPR values inside and immediately proximal to the crater (R<~1.5) have not yet reverted to the background CPR of the maria; the upper interior slopes particularly remain elevated in CPR, consistent with the idea that this area has thin regolith because it is an area of net erosion.

Discussion: *Comparison to DIVINER:* Qualitatively, the CPR evolution around craters agrees well with DIVINER observations of rock abundances around young craters [3,15]. The fact that the rockiness of the ejecta deposit at the surface becomes indistinguishable from background values over a ~Ga timescale agrees reasonably with earlier estimates [3], although CPR values may stay elevated longer than the thermal signatures remain anomalous for the same size craters. This is consistent with earlier suggestions that rocks survive in the subsurface longer than they survive on the surface [4,15,16].

Comparison to earlier observations of CPR evolution: Earlier work [17] has reported no clear evolution of craters' CPR with time, contrary to our results. However, this earlier work was generally based on observations of far fewer craters of much larger diameter. The ejecta of large craters evolves more slowly [2,7,9] than the km-scale craters described here. In addition, the results in Fig. 2 required combination of a very large number of observations to reduce natural variability and speckle noise inherent in the radar data. It is possible that applying this approach for larger craters may reveal some evolutionary pattern at larger sizes as well.

Usefulness for chronology: Because the CPR signature of kilometer-scale craters evolves in a distinctive way, it has potential usefulness as proxy for age. Note that, for any individual crater (e.g., Fig. 1), with current data, this may be a relatively weak proxy. Nonetheless, by combining observations of rock abundance [3], topographic degradation [13], optical maturity [18], and crater statistics [20], it may be possible to derive a more accurate age estimate for individual craters than application of any of these methods alone.

References: [1] Gault D.E. et al. (1974), *Proc. LPSC, 5*, 2365-2386. [2] Thompson, T.W. et al. (1981), *Icarus*, *46*, 201-225. [3] Ghent R. R. et al. (2014), *Geology*, *42*, 1059-1062. [4] Basilesvky, A.T. et al. (2013), *PSS*, *89*, 118-126. [5] Bart, G.D., Melosh, H.J., (2010), *Icarus*, *209*, 337-357. [6] Stopar, J.D. et al. (2014), *Icarus*, *243*, 337-357. [7] Thomson, B. J. et al. (2013), *LPSC 44*, 2107. [8] Ghent, R.R. et al. (2005), *JGR*, *110*, E20005. [9] Bell, S.W. et al. (2012), *JGR*, *117*, E00H30. [10] Nozette, S. et al. (2010), *Space Sci. Rev.*, *150*, 285-302. [11] Cahill, J.T.S. et al. (2014), *Icarus*, *243* 173-190. [12] Campbell, B.A. et al. (2010), *Icarus*, *208*, 565–573. [13] Fassett, C.I., Thomson, B.J. (2014), *JGR-P.*, *119*, 2255–2271. [14] Krishna, N, Kumar, P.S. (2016), *Icarus*, *264*, 274–299. [15] Bandfield, J.L. et al. (2011), *JGR*, *116*, E00H02. [16] Ghent, R.R. et al. (2016), *273*, 182–195. [17] Ghent, R.R. et al. (2016), *New Views 2*, 6040. [18] Grier, J. A. et al. (2001), *JGR*, 106, 32847–32862. [19] Hiesinger, H. et al. (2012), *JGR*, *117*, E00H10.

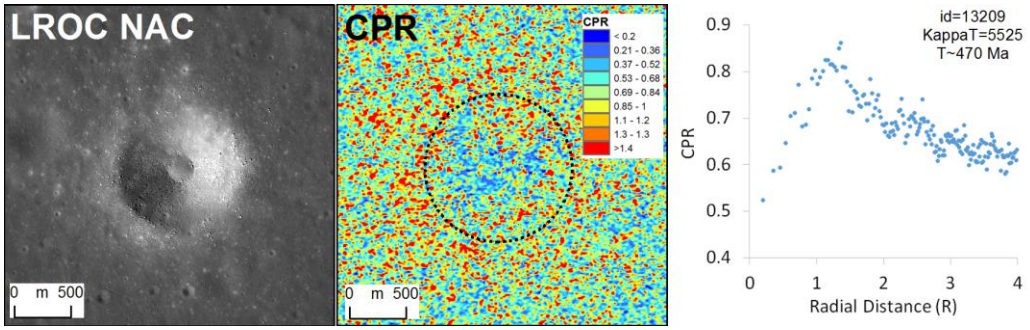

Fig. 1. Example of a relatively fresh 1.2-km crater in LROC image M183404026, with CPR data from Mini-RF swath lsz_01385_2cp_eku_29n019_v1. The radial profile is a 500-point median of the nearest CPR observations in radial distance.

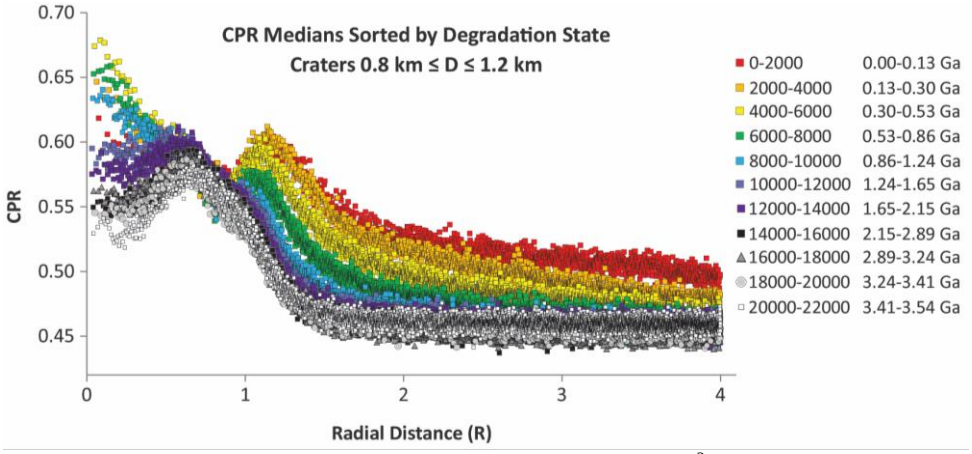

Fig. 2. Grouped, median profiles of craters in different degradation state (κt in 2000 m^2 bins; age estimates for each group are given, following [13]). The profiles are 5000-point median values of the nearest CPR observations in radial distance. The x-axis is the distance from crater center normalized by the craters radius, so R=1 is the observed topographic rim.